

*Supplementary Materials for*

**Anchoring Co-Fe alloy nano-grains on carbon fibers by in-situ alloying strategy to boost the catalytic performance for rapid oxidative degradation of emerging contaminants**

Man Yang<sup>a,b,1</sup>, Xianghan Cheng<sup>a,1</sup>, Fengting Geng<sup>a</sup>, Wenyuan Han<sup>a</sup>, Ping Niu<sup>a</sup>, Long Xie<sup>b</sup>, Zhen Li<sup>a</sup>, Yong-Zheng Zhang<sup>a\*</sup>, Da-Shuai Zhang<sup>a</sup>, Jing Xu<sup>a\*</sup>, Xiuling Zhang<sup>a</sup>, Longlong Geng<sup>a\*</sup>

<sup>a</sup> *Shandong Provincial Key Laboratory of Monocrystalline Silicon Semiconductor Materials and Technology, College of Chemistry and Chemical Engineering, Dezhou University, Dezhou 253023, P. R. China.*

<sup>b</sup> *School of Chemical Engineering and Technology, North University of China, Taiyuan 030051, P. R. China*

<sup>1</sup> These authors contributed equally.

\*Corresponding authors:

E-mail Addresses: [zhangyongzheng23@163.com](mailto:zhangyongzheng23@163.com) (Y.-Z. Zhang),  
[xujing2306@163.com](mailto:xujing2306@163.com) (J. Xu) and [llgeng@126.com](mailto:llgeng@126.com) (L. Geng).

## 1. Experimental section

### 1.1 Materials and reagents

Ferric nitrate hydrate ( $\text{Fe}(\text{NO}_3)_3 \cdot 9\text{H}_2\text{O}$ ) and hydrochloric acid (HCl) were purchased from Sinopharm Chemical Reagent Co. Cobalt nitrate hexahydrate ( $\text{Co}(\text{NO}_3)_2 \cdot 6\text{H}_2\text{O}$ ) was purchased from Tianjin Damao Chemical Reagent Factory. Sodium hydroxide (NaOH) and anhydrous ethanol ( $\text{CH}_3\text{CH}_2\text{OH}$ ) were purchased from Xilong Science Co. Sodium carbonate ( $\text{Na}_2\text{CO}_3$ ), methyl orange ( $\text{C}_{14}\text{H}_{14}\text{N}_3\text{NaO}_3\text{S}$ ) and anhydrous sodium sulfate ( $\text{Na}_2\text{SO}_4$ ) were purchased from Tianjin Beifang Tianming Chemical Reagent Factory. Sodium dihydrogen phosphate dihydrate ( $\text{NaH}_2\text{PO}_4 \cdot 2\text{H}_2\text{O}$ ), L-histidine ( $\text{C}_6\text{H}_9\text{N}_3\text{O}_2$ ), tert-butanol ( $\text{C}_4\text{H}_{10}\text{O}$ ), oxytetracycline ( $\text{C}_{22}\text{H}_{24}\text{N}_2\text{O}_9$ ), acid orange 7 ( $\text{C}_{16}\text{H}_{11}\text{N}_2\text{NaO}_4\text{S}$ ), rhodamine B ( $\text{C}_{28}\text{H}_{31}\text{ClN}_2\text{O}_3$ ), p-benzoquinone ( $\text{C}_6\text{H}_4\text{O}_2$ ), tetracycline ( $\text{C}_{22}\text{H}_{24}\text{N}_2\text{O}_8$ ) and phenazine methosulfate ( $\text{C}_{14}\text{H}_{14}\text{N}_2\text{O}_4\text{S}$ ) were purchased from Shanghai McLean Biochemical Technology Co. Sodium chloride (NaCl) and sodium bicarbonate ( $\text{NaHCO}_3$ ) were purchased from Tianjin Yongda Chemical Reagent Development Centre. Methylene blue ( $\text{C}_{16}\text{H}_{18}\text{ClN}_3\text{S} \cdot 3\text{H}_2\text{O}$ ) was purchased from Tianjin Hengxing Chemical Reagent Manufacturing Co. Skimmed cotton was purchased from Shandong Bangdun Medical Technology Co. Distilled water was used throughout the study.

### 1.2 Catalysts preparation

The CoFe/CF catalyst was prepared through a two-step procedure involving a wet impregnation and temperature-controlled pyrolysis process, as illustrated in the synthesis scheme in Fig. 1a. The typical steps were as follows: 0.1428 g  $\text{Co}(\text{NO}_3)_2 \cdot 6\text{H}_2\text{O}$ , 0.1980 g

$\text{Fe}(\text{NO}_3)_3 \cdot 9\text{H}_2\text{O}$  and 3.0 g cotton fibre were added to 300 mL of deionized water and stirred for 1 hour. Then, the pH of the suspension was adjusted to 11 using sodium hydroxide solution (1 mol/L) and stirred for 1 hour. Subsequently, the solids were filtered, washed repeatedly with deionized water and dried at 100°C for 12 h. Finally, the precursors were thermally treated in a tube furnace for 3 h in a nitrogen flow, and the obtained catalysts were denoted as CoFe/CF-x, where x represented as the temperature. For comparison, carbon fibers were also synthesized by thermal treating cotton fibers at 800°C for 3 h, and the sample was designated as CF-800.

### 1.3 Catalysts characterization

A field emission scanning electron microscope (SEM, MERLIN Compact) and a transmission electron microscope (TEM, FEI Tecnai F20) were employed to observe the morphological features of the materials. The fresh and used catalysts were studied by a powder X-ray diffractometer (XRD, D8 ADVANCE). The valence states of C, O, Co and Fe in CoFe/CF-800 were analyzed by X-ray photoelectron spectroscopy (XPS, Thermo Scientific K-Alpha). The surface chemistry of the materials was analyzed by Fourier transform infrared spectroscopy (FTIR, Nicolet IS50). X-ray absorption spectra (XAS) were collected at the Shanghai Synchrotron Radiation Facility (SSRF), which is equipped with a third-generation synchrotron radiation source and an electron accelerator with a luminous energy of 150 MeV. Extended X-ray absorption fine structure (EXAFS) of Co K-edge and Fe K-edge was obtained by  $k^3$ -weighted Fourier transform. The specific surface area and pore structure were quantified using a gas adsorption analyzer (BSD-PMC). The absorbance of TC was determined using a Shimadzu UV-2700 spectrometer. Magnetic measurements were performed with a vibrating

sample magnetometer (Impulse VSM-400) at room temperature under a magnetic field of 40000 ohm. The inductively coupled plasma emission spectrometer (Thermofisher CPA PRO) was employed to ascertain the leaching of Co and Fe ions subsequent to the utilization of CoFe/CF-800. The principal active substances were identified utilizing electron paramagnetic resonance (EPR, Bruker EMXplus-6/1). The intermediates of TC degradation were monitored using high-performance liquid chromatography-quadrupole time-of-flight mass spectrometry (Q-TOF 6530) (LC-MS). A 5 mL sample solution was collected and 100  $\mu$ L of sodium thiosulfate solution was immediately added to terminate the reaction, which was quenched by the addition of methanol and immediately filtered through a 0.22  $\mu$ m filter membrane for LC-MS determination. The mobile phase consisted of eluent A, a 0.1% formic acid aqueous solution (V/V), and eluent B, acetonitrile (chromatographically pure). The flow rate was 0.2 mL/min, and the injection volume was 5  $\mu$ L. The gradient solvents were as follows: A = 90% (0 min), 10% (10 min), 10% (14 min), 90% (15 min), and 90% (16 min). The spray voltage was 3.0 kV for positive ions, and the scanning range was 100-800 m/z.

#### **1.4 Catalytic activity measurements**

The reaction was typically carried out in a 250 ml beaker containing TC solution (20 mg/L, 100 mL), with the adsorption-desorption equilibrium established by the addition of catalyst (10 mg) (15 min), followed by the addition of PMS, which was placed in a thermostatic water bath at 25°C to initiate the oxidation process. The effects of the following parameters on TC degradation were investigated. The parameters investigated included the dosage of CoFe/CF-800 (0.005 g, 0.01 g and 0.02 g), the dosage of PMS (0.01g, 0.02g and 0.03 g). In

addition, the initial pH (3, 5, 7, 9, and 11), and the coexisting ions ( $\text{Cl}^-$ ,  $\text{CO}_3^{2-}$ ,  $\text{HCO}_3^-$ ,  $\text{SO}_4^{2-}$ ,  $\text{H}_2\text{PO}_4^-$ ) were considered. The initial pH was adjusted with 0.1 M HCl and 0.1 M NaOH. Samples were collected at set time points using a plastic syringe, with 3 mL of solution filtered through a 0.22  $\mu\text{m}$  PES membrane. The absorbance of TC was measured at 360 nm using a UV-Vis spectrophotometer. The initial concentration of other contaminants (OTC, MB, MO, AO7, RhB) was designed to be 20 mg/L. CoFe/CF-800 was not recovered in the cycling test. The addition of CoFe/CF-800 (0.01 g) to a 250 ml beaker containing TC (20 mg/L, 100 ml) and PMS (0.02 g) was typically employed to initiate the reaction. CoFe/CF-800 was separated with a magnet, washed with deionized water and dried at 80°C. The dried catalyst was then used for the next reaction. All experiments were conducted in triplicate to eliminate potential errors. In the burst experiments, ethanol ( $\text{SO}_4^{\bullet-}$  and  $\bullet\text{OH}$ ), TBA ( $\text{SO}_4^{\bullet-}$ ), *p*-benzoquinone ( $\text{O}_2^{\bullet-}$ ), and L-histidine ( $^1\text{O}_2$ ) were selected as the bursting agents to remove the corresponding reactive species. The reactive oxygen species generated during catalysis were investigated using electron paramagnetic resonance. The intermediates of TC degradation were examined by LC-MS in order to infer the possible degradation pathways of TC.

### 1.5 Reaction kinetics calculation

Since the amount of oxidant (PMS) is much higher than that of TC during the reaction, and therefore a pseudo-first-order kinetic model was carried out to evaluate the oxidation kinetics of different catalysts using the equation:

$$\ln \left( A_t / A_0 \right) = -k t$$

To further confirm the primary ROSs in TC elimination, the rate constant (*k*) could be

used to examine the contribution ratios of diverse ROS types to TC degradation. It was possible to determine the contributions of ROSs using the method outlined above, taking into account that the TC oxidization process in CoFe/CF-800/PMS system was correlated well with the pseudo-first-order kinetic model. Eq. 1 was used to calculate the contribution ratios of  $\bullet\text{OH}$ ,  $\text{O}_2^{\bullet-}$  and  $^1\text{O}_2$ . Eq. 2 was employed to compute the contribution ratios of  $\text{SO}_4^{\bullet-}$  contribution ratio.

$$\text{Relative contribution of ROSs} = \frac{k_{obs} - k_{obs}(\text{scavenger})}{k_{obs}} \times 100\% \quad (1)$$

$$\text{Relative contribution of sulfate radical} = \frac{k_{obs}(\text{TBA}) - k_{obs}(\text{EtOH})}{k_{obs}} \times 100\%$$

(2)

## 1.6 Theory calculations

All spin-polarized density-functional theory (DFT) computations were performed using the Vienna ab initio simulation package (VASP) based on the projector augmented wave (PAW) method. Electron-ion interactions were described using standard PAW potentials. A plane-wave basis set was employed to expand the smooth part of the wave functions with a cutoff kinetic energy of 400 eV. For the Electron-electron exchange and correlation interactions, the functional parametrized by Perdew-Burke-Ernzerhof (PBE), a form of the general gradient approximation (GGA), was used throughout. The Van der Waals interaction was described via the DFT-D3BJ method. To study the mechanistic chemistry of surface reactions, the surface was modelled with a slab model. A sufficiently large vacuum region of 15 Å was used to ensure the periodic images were well separated. During the geometry

optimizations, the bottom atoms were fixed at the bulk position when the surface properties were calculated. In this work, the Brillouin-zone integrations were conducted using Monkhorst-Pack grids of special points with a separation of  $0.06 \text{ \AA}^{-1}$ . The convergence criterion for the electronic self-consistent loop was set to  $10^{-5} \text{ eV}$ . The atomic structures were optimized until the residual forces were below  $0.03 \text{ eV \AA}^{-1}$ .

## 2. Characterization results

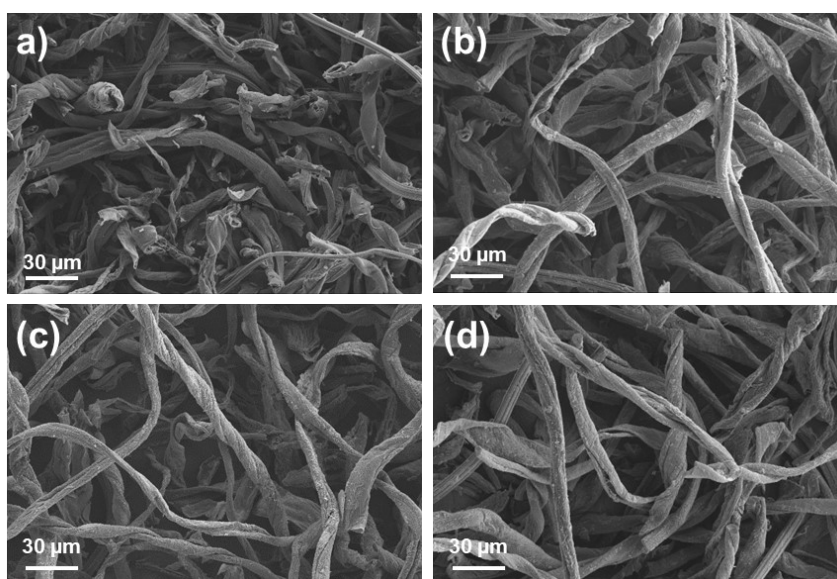


**Fig. S1** SEM images of CF-800 (a), CoFe/CF-800 (b), CoFe/CF-600 (c), CoFe/CF-400 (d).

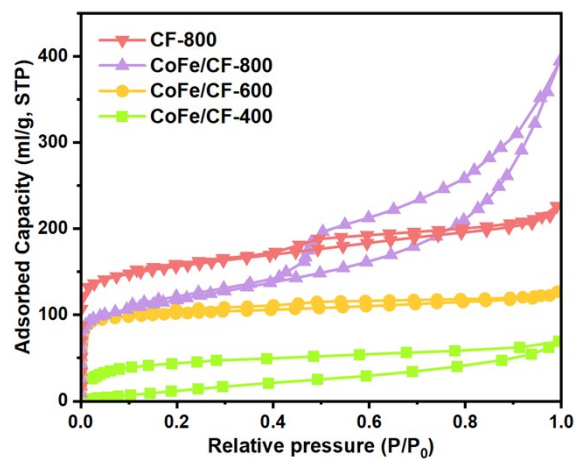


**Fig. S2** Nitrogen adsorption-desorption curves of CF-800, CoFe/CF-800, CoFe/CF-600 and CoFe/CF-400.

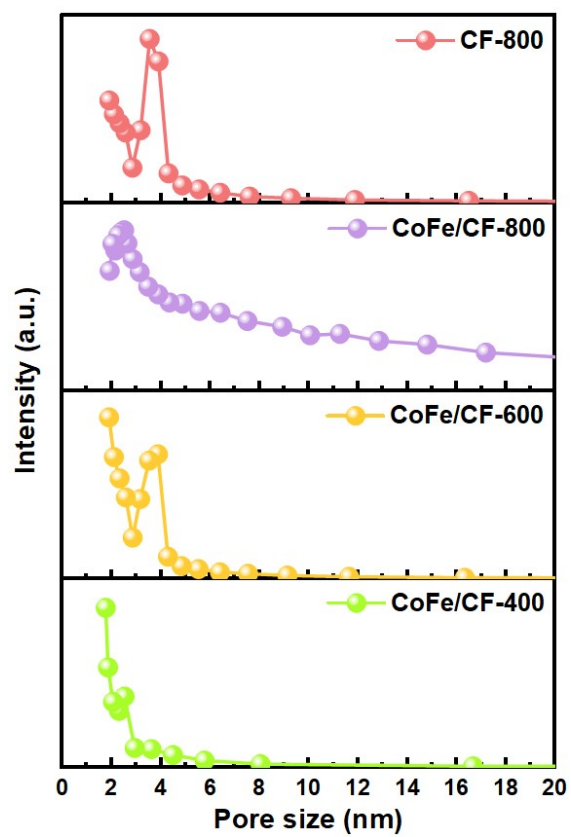


**Fig. S3** Pore size distribution signals of CF-800, CoFe/CF-800, CoFe/CF-600 and CoFe/CF-400.

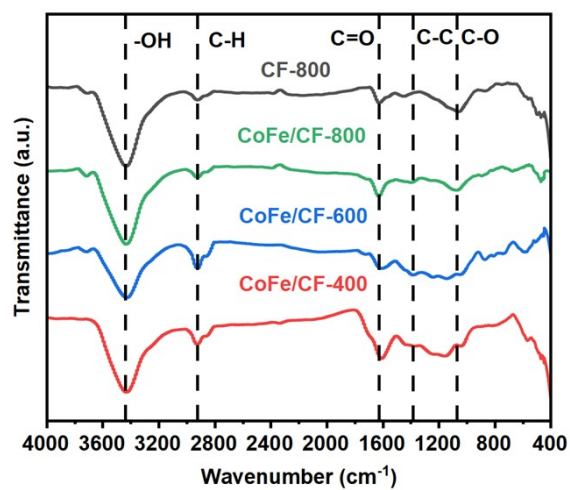


**Fig. S4** FTIR spectra of CF-800 and CoFe/CF catalysts.

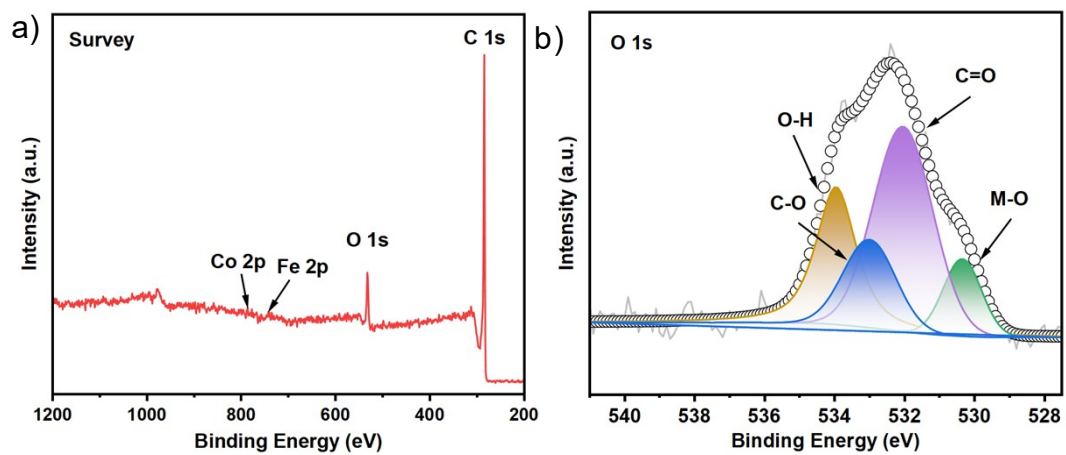


**Fig. S5** XPS spectra of survey (a) and O 1s (b) of CoFe/CF-800.

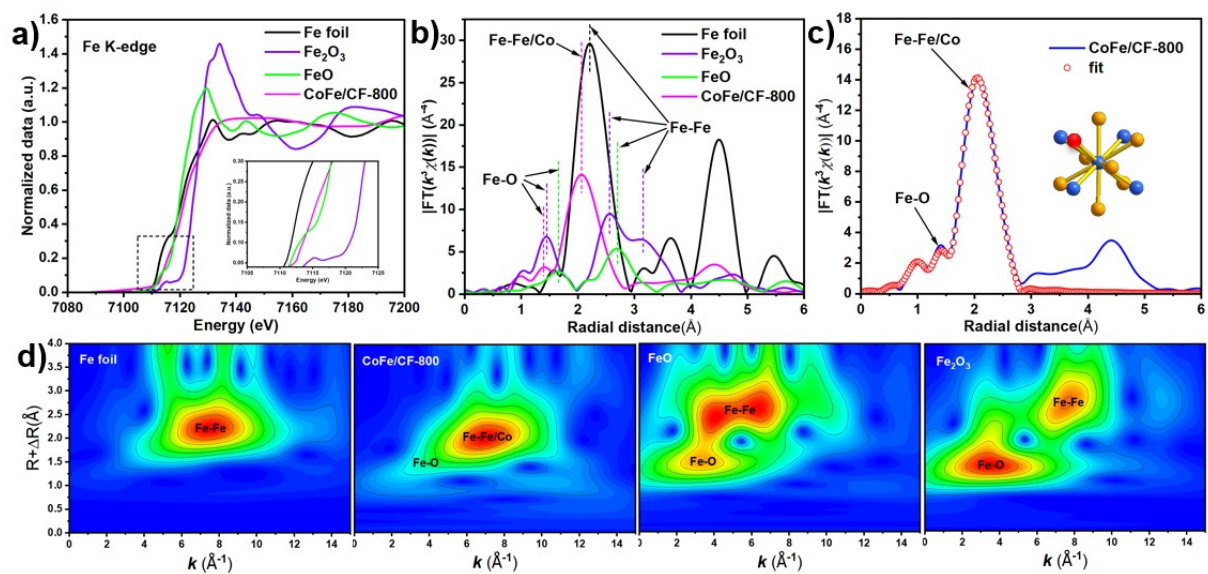


**Fig. S6** X-ray absorption spectra of CoFe/CF-800 and reference sample including Fe foil,  $\text{Fe}_2\text{O}_3$ , FeO: XANES spectra (a), Fourier transform of Fe K-edge EXAFS of different samples (b), EXAFS fitting curve of CoFe/CF-800 in R-space (c) and wavelet transforms for the EXAFS signals of different Fe-based samples (d).

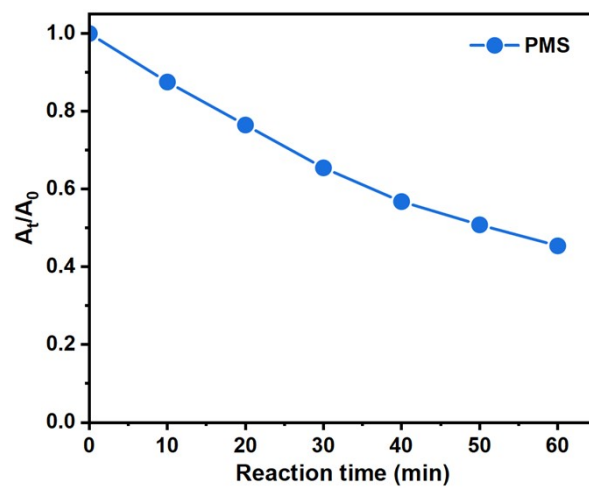


**Fig. S7** The TC catalytic degradation activity in the sole PMS system.

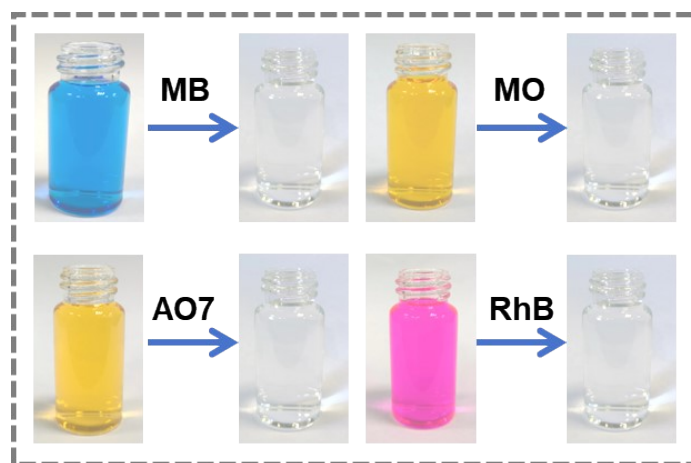


**Fig. S8** Colour change before and after dye degradation.

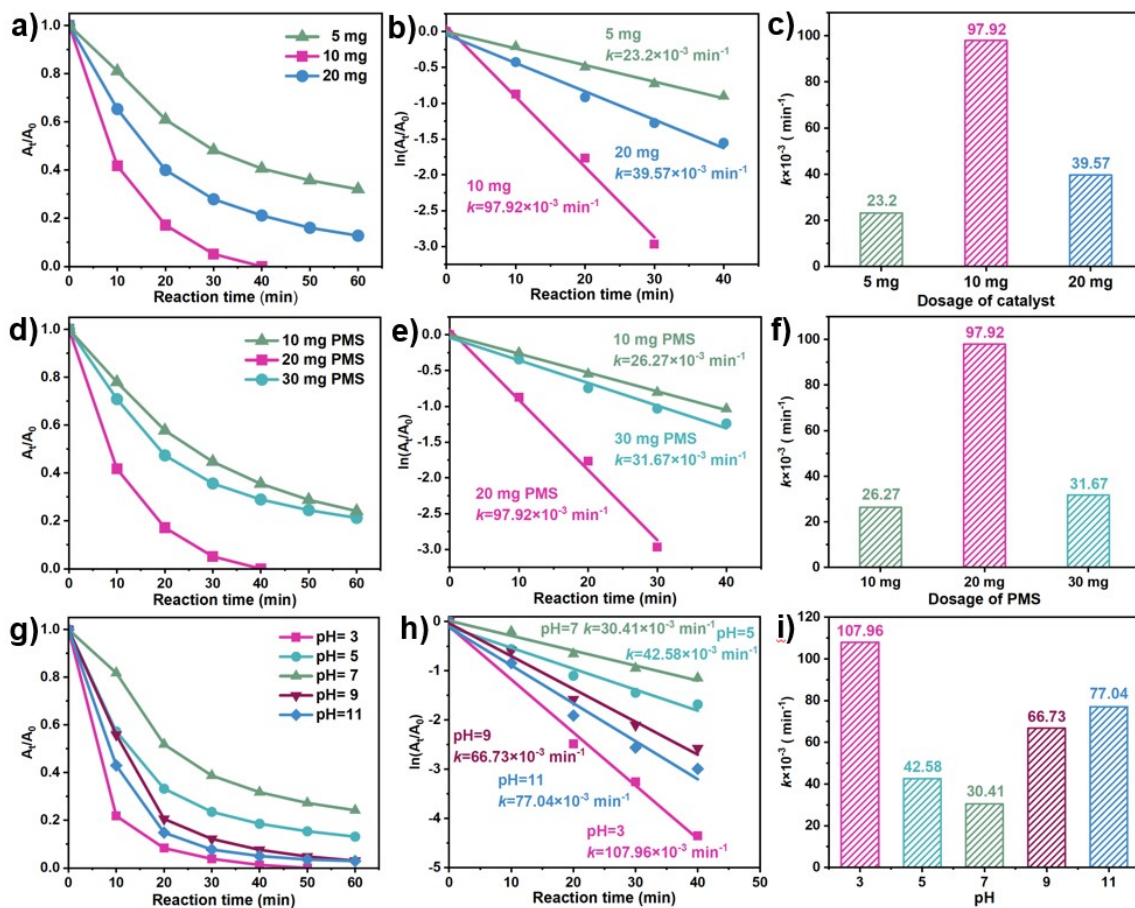


**Fig. S9** Effect of reaction parameters on the catalytic behavior of CoFe/CF-800 for TC degradation: catalyst dosage (a-c), PMS dosage (d-f) and initial pH (g-i).

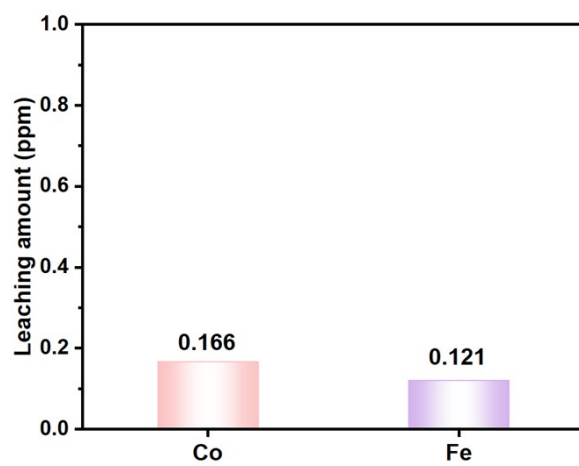


**Fig. S10** The leaching amount of cobalt ion and iron ion in the CoFe/CF-800/PMS system.

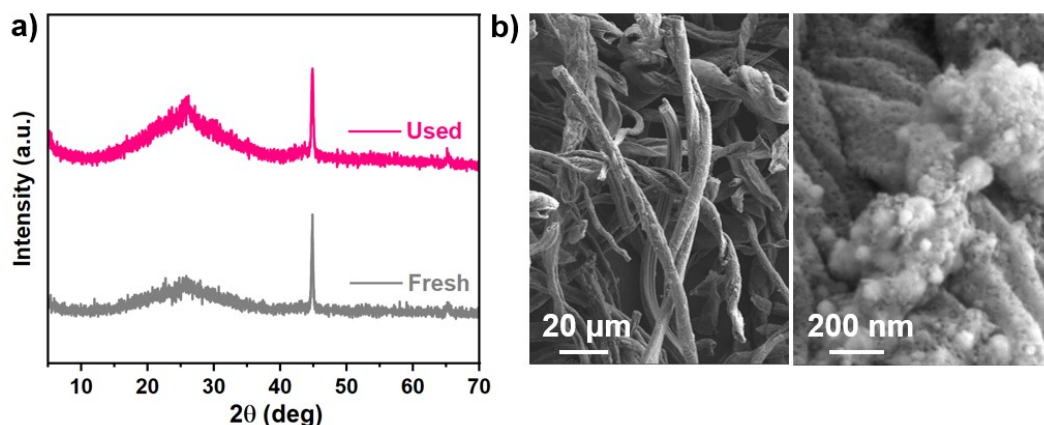


**Fig. S11** XRD patterns of CoFe/CF-800 before and after the reactions (a). SEM image of used CoFe/CF-800 catalysts (b).

To further investigate the stability of the catalyst, SEM (Fig. S9) analyses were conducted. No obvious changes in the morphology were observed for the catalyst before and after the reaction. Furthermore, it can be observed from the XPS spectra (Fig. S10a-b) of CoFe/CF-800 after the reaction that the proportions of Co(0) and Fe(0) are slightly reduced and high-valence species are slightly increased, indicating that redox reactions occurred between these active species and PMS. Although Co(0) and Fe(0) cannot be regenerated, there were two redox cycles of  $\text{Fe}^{2+} \leftrightarrow \text{Fe}^{3+}$  and  $\text{Co}^{2+} \leftrightarrow \text{Co}^{3+}$  in the system to ensure that CoFe/CF-800 would not be completely deactivated, retaining good stability. In summary, the stability of CoFe/CF-800 was significantly verified, confirming its good potential for practical applications.

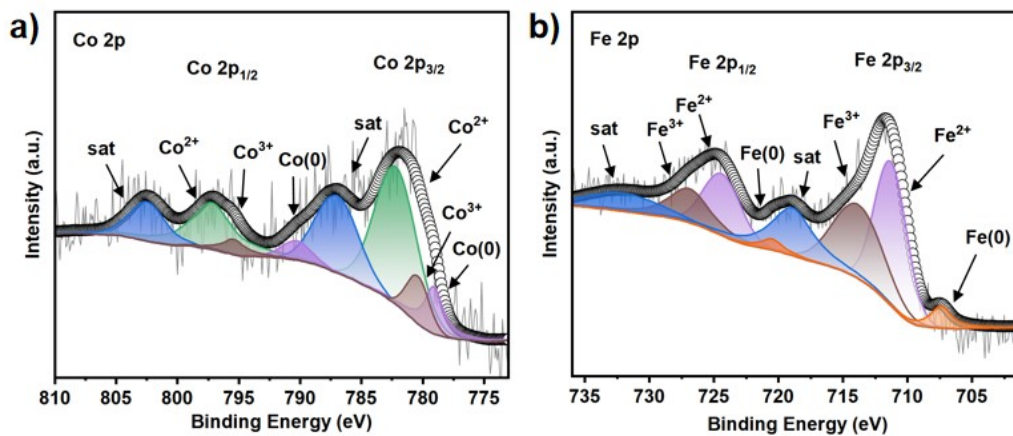


**Fig. S12** High resolution XPS spectra Co 2p (a), Fe 2p (b) of used CoFe/CF-800.

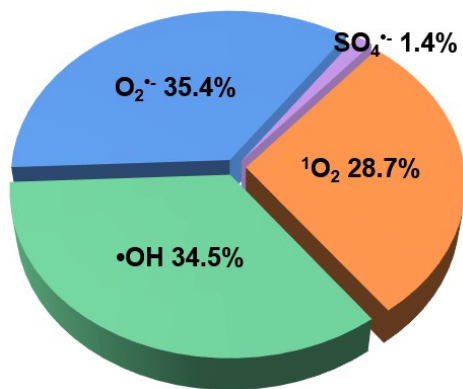


**Fig. S13** The contribution of ROSs during TC degradation process.

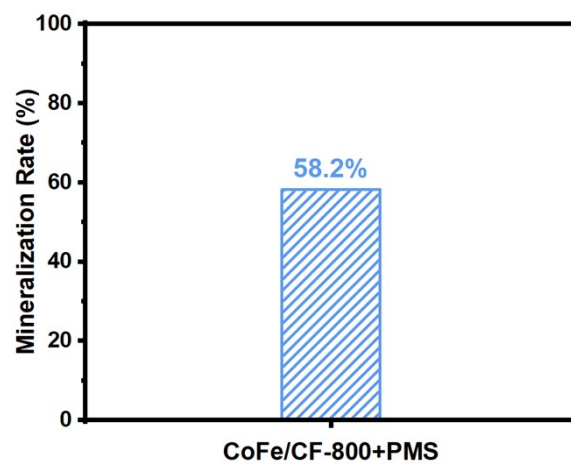


**Fig. S14** Mineralization rate of TC in the CoFe/CF-800/PMS system.

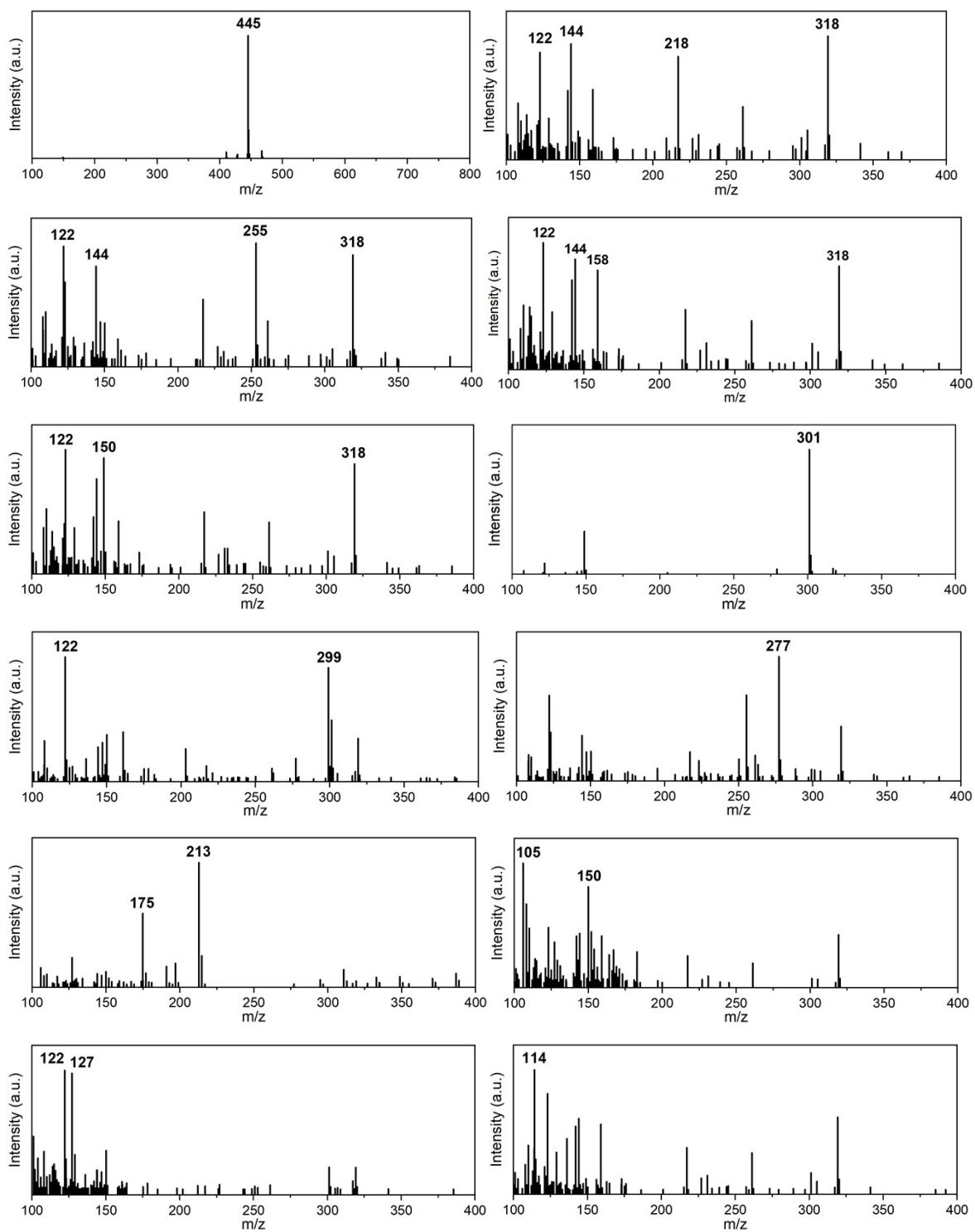


**Fig. S15** LC-MS spectra of the TC and intermediates.

**Table S1.** Structural properties of the obtained catalysts.

Sample	Specific Surface Area (m <sup>2</sup> /g)	Pore Volume (cm <sup>3</sup> /g)	Pore Size (nm)
CF-800	499.8	0.17	3.5
CoFe/CF-800	389.3	0.51	3.8
CoFe/CF-600	319.3	0.06	1.8
CoFe/CF-400	51.2	0.12	1.7

**Table S2.** EXAFS data fitting results of Samples.

Sample	Path	CN <sup>a</sup>	R(Å) <sup>b</sup>	$\sigma^2$ (Å <sup>2</sup> ) <sup>c</sup>	$\Delta E_0$ (eV) <sup>d</sup>	R factor
Fe K-edge ( $S_0^2=0.876$ )						
Fe foil	Fe-Fe	8*	2.464±0.008	0.0045	5.4	0.0019
	Fe-Fe	6*	2.851±0.009	0.0051		
FeO	Fe-O	6.0±0.1	2.121±0.016	0.0090	3.8	0.0058
	Fe-Fe	11.9±0.3	3.074±0.011	0.0087	1.5	
Fe <sub>2</sub> O <sub>3</sub>	Fe-O	5.9±0.2	1.947±0.014	0.0039	-0.8	0.0018
	Fe-Fe	6.2±0.2	2.968±0.009	0.0075	-0.2	
	Fe-Fe	4.7±0.3	3.453±0.017		3.4	
	Fe-Fe	4.5±0.7	3.742±0.018		2.3	
CoFe/CF-800	Fe-O	1.0±0.2	1.621±0.011	0.0010	-7.6	0.0028
	Fe-Co	7.1±0.4	2.420±0.011	0.0099	-9.5	
	Fe-Fe	3.9±0.6	2.773±0.009			
Co K-edge ( $S_0^2=0.811$ )						
Co foil	Co-Co	12*	2.494±0.003	0.0065	8.1	0.0025
CoO	Co-O	6.1±0.3	2.126±0.015	0.0078	0.1	0.0015
	Co-Co	11.8±0.5	3.005±0.012	0.0141	-5.1	
Co <sub>3</sub> O <sub>4</sub>	Co-O	5.9±0.3	1.920±0.007	0.0020	-6.1	0.0034
	Co-Co	6.1±0.5	2.867±0.010	0.0040	-5.9	
	Co-Co	7.4±0.8	3.336±0.013		-2.4	
CoFe/CF-800	Co-O	0.8±0.2	1.908±0.014	0.0025	-5.0	0.0067
	Co-Fe	7.1±0.3	2.442±0.011	0.0089	-5.4	
	Co-Co	3.5±0.6	2.789±0.010			

<sup>a</sup>CN, coordination number; <sup>b</sup>R, the distance between absorber and backscatter atoms; <sup>c</sup> $\sigma^2$ , the Debye Waller factor value; <sup>d</sup> $\Delta E_0$ , inner potential correction to account for the difference in the inner potential between the sample and the reference compound; R factor indicates the goodness of the fit.  $S_0^2$  was fixed to 0.876 and 0.811, according to the experimental EXAFS fit of Fe foil and Co foil by fixing CN as the known crystallographic value. \* This value was fixed during EXAFS fitting, based on the known structure of Fe and Co. Fitting conditions:  $k$  range: 2.0 - 12.0;  $R$  range: 1.0 - 3.0; fitting space: R space;  $k$ -weight = 3. A reasonable range of EXAFS fitting parameters:  $0.800 < S_0^2 < 1.000$ ;  $CN > 0$ ;  $\sigma^2 > 0 \text{ \AA}^2$ ;  $|\Delta E_0| < 10 \text{ eV}$ ;  $R$

factor < 0.02.

**Table S3.** Comparison of rate constant of PMS activation for organic pollutants degradation on different heterogeneous catalysts.

Catalysts	Catalyst dosage	Pollutant solution	PMS dosage	Reaction time	Efficiency (%)	Reaction rate	Ref.
CoFe/CF-800	10 mg	20 mg L <sup>-1</sup> (100 mL)	20 mg	55 min	100	0.098 min <sup>-1</sup>	This work
Co <sub>3</sub> O <sub>4</sub> /CPANI	0.15 g/L	20 mg L <sup>-1</sup> (100 mL)	0.15 g/L	40 min	92.1%	0.090 min <sup>-1</sup>	1
LaCoO <sub>3</sub> -g-C <sub>3</sub> N <sub>4</sub>	0.2 g/L	20 mg L <sup>-1</sup> (50 mL)	0.1 g/L	30 min	69.8%	0.032 min <sup>-1</sup>	2
LFNO-5	20 mg	20 mg L <sup>-1</sup> (100 mL)	0.018 g/L	90 min	90.0%	0.034 min <sup>-1</sup>	3
FONC@PAC	0.5 g/L	150 mg L <sup>-1</sup> (150 mL)	5 mM	60min	86.9%	0.030 min <sup>-1</sup>	4
MCN	100 mg/L	20 mg L <sup>-1</sup>	0.5 g/L	60 min	80.0%	0.028 min <sup>-1</sup>	5
pyrite	1 g/L	50 mg L <sup>-1</sup> (50 mL)	1 g/L	45 min	100%	0.086 min <sup>-1</sup>	6
MoS <sub>2</sub> /Ag/g-C <sub>3</sub> N <sub>4</sub>	20 mg	20 mg L <sup>-1</sup> (100 mL)	0.1 mM	50 min	98.9%	0.084 min <sup>-1</sup>	7
CoFe <sub>2</sub> O <sub>4</sub> /TNTs	10 mg	100 mg L <sup>-1</sup> (50 mL)	4 g/L	60 min	97.0%	0.067 min <sup>-1</sup>	8
MIL-88A	25 mg	200mg L <sup>-1</sup> (100 mL)	4 mM	70 min	100%	0.040 min <sup>-1</sup>	9
CuFe <sub>2</sub> O <sub>4</sub> -CoFe <sub>2</sub> O <sub>4</sub>	0.2 g/L	20 mg L <sup>-1</sup> (100 mL)	0.3 g/L	130 min	99.3%	0.051 min <sup>-1</sup>	10

**Table S4.** The second-order rate constants for the reaction of test quenchers with  $\bullet\text{OH}$ ,  $\text{SO}_4^{\bullet-}$ ,  $\text{O}_2^{\bullet-}$ , and  $^1\text{O}_2$ .

Reaction rate constant ( $\text{M}^{-1} \text{S}^{-1}$ )				
Chemicals	$k_{\bullet\text{OH}}$	$k_{\text{SO}_4^{\bullet-}}$	$k_{^1\text{O}_2}$	$k_{\text{O}_2^{\bullet-}}$
Ethanol	$2.8 \times 10^9$ <sup>11</sup>	$7.7 \times 10^7$ <sup>12</sup>	$3.8 \times 10^3$ <sup>13</sup>	---
Tert-butanol	$6.0 \times 10^8$ <sup>11</sup>	$4 \times 10^5$ <sup>12</sup>	$3.04 \times 10^3$ <sup>13</sup>	No reaction <sup>14</sup>
L-histidine	$7.1 \times 10^9$ <sup>15</sup>	$2.5 \times 10^9$ <sup>12</sup>	$3.2 \times 10^7$ <sup>16</sup>	---
<i>p</i> -Benzoquinone	$1.2 \times 10^9$ <sup>17</sup>	---	$3.4 \times 10^7$ <sup>17</sup>	$8.3 \times 10^8$ <sup>17</sup>

## Reference

1. J. Qian, X. Mi, Z. Chen, W. Xu, W. Liu, R. Ma, Y. Zhang, Y. Du and B.-J. Ni, *J. Cleaner Prod.*, 2023, **405**, 137023.
2. X. Yuan, Y. Leng, C. Fang, K. Gao, C. Liu, J. Song and Y. Guo, *New J. Chem.*, 2022, **46**, 12217-12228.
3. N. He, Z. Yu, G. Yang, J. Wang, Q. Tan and Y. Liu, *J. Mol. Liq.*, 2023, **389**, 122883.
4. J. Zhou, X. Li, J. Yuan and Z. Wang, *Chem. Eng. J.*, 2022, **441**, 136061.
5. H. Shi, Y. He, Y. Li, T. He and P. Luo, *Sep. Purif. Technol.*, 2022, **280**, 119864.
6. F. Rahimi, J. P. van der Hoek, S. Royer, A. Javid, A. Mashayekh-Salehi and M. Jafari Sani, *J. Water Process Eng.*, 2021, **40**, 101808.
7. C. Jin, J. Kang, Z. Li, M. Wang, Z. Wu and Y. Xie, *Appl. Surf. Sci.*, 2020, **514**, 146076.
8. Y. Du, W. Ma, P. Liu, B. Zou and J. Ma, *J. Hazard. Mater.*, 2016, **308**, 58-66.
9. Y. Zhang, J. Zhou, X. Chen, L. Wang and W. Cai, *Chem. Eng. J.*, 2019, **369**, 745-757.
10. Z. Li, F. Wang, Y. Zhang, Y. Lai, Q. Fang and Y. Duan, *Chem. Eng. J.*, 2021, **423**, 130093.
11. G. V. Buxton, C. L. Greenstock, W. P. Helman and A. B. Ross, *J. Phys. Chem. Ref. Data*, 1988, **17**, 513-886.
12. P. Neta, R. E. Huie and A. B. Ross, *J. Phys. Chem. Ref. Data*, 1988, **17**, 1027-1284.
13. M. A. J. Rodgers, *J. Am. Chem. Soc.*, 1983, **105**, 6201-6205.
14. Y. Guo, J. Long, J. Huang, G. Yu and Y. Wang, *Water Res.*, 2022, **215**, 118275.
15. M. A. Babizhaye, M. C. Seguin, J. Gueyne, R. P. Evstigneeva, E. A. Ageyeva and G. A. Zheltukhina, *Biochem. J.*, 1994, **304**, 509-516.

16. L. Gao, Y. Guo, J. Zhan, G. Yu and Y. Wang, *Water Res.*, 2022, **221**, 118730.

17. P. S. Rao and E. Hayon, *J. Phys. Chem.*, 1975, **79**, 397-402.